PRESSURE-DRIVEN ERUPTION OF LIQUID RESERVOIRS IN TITAN'S ICE SHELL

A FINAL REPORT SUBMITTED TO THE DEPARTMENT OF EARTH SCIENCES, UNIVERSITY OF HAWAIʻI AT MĀNOA, IN PARTIAL FULLFILMENT OF THE REQUIRONMENTS FOR THE DEGREE OF

MASTER OF SCIENCE

IN

EARTH AND PLANETARY SCIENCES

DECEMBER 2020

BY

GWENDOLYN BROUWER

COMMITTEE:

SARAH FAGENTS (CHAIR)

BRIDGET SMITH-KONTER

GARRETT APUZEN-ITO

Abstract

Titan's organic-rich atmosphere and subsurface water ocean make it a target of interest in the search for extraterrestrial life. To investigate Titan's habitability, it is important to identify mechanisms for transfer of potential biosignatures from the ocean to the surface where they might be detected by future missions. In this study we model the ascent of liquid water through a fracture due to the pressurization caused by progressive freezing of liquid in a spherical subsurface reservoir within Titan's ice shell. By extending a pressure-driven eruption model that has been applied to resurfacing on Europa, we calculate the volume fraction of the reservoir that needs to freeze to generate the critical reservoir pressure to produce an eruption, and the time required for that degree of freezing to be achieved as a function of reservoir depth and volume. We explore spherical reservoirs with radii between 100 and 5000 m containing four possible cryomagma compositions; pure liquid water, aqueous ammonia with 1.5 wt.% ammonia, and aqueous ammonium sulfate with 10 wt.% and 20 wt.% ammonium sulfate. For reservoirs between the surface and 30 km depth in Titan's ice shell, we find that 1 – 32% of the cryomagma in the reservoirs must freeze to cause an eruption, taking months to the order of 10^4 years. We find the volume of erupted materials to be between 10^4 – 10^{10} m^3, comparable to volumes of observed potential cryovolcanic flow features on Titan (10^6 – 10^{11} m^3). The results of this modeling study therefore support the feasibilty of pressure-driven eruption through Titan's ice shell.

1 Introduction

Saturn's moon Titan is the only satellite in the solar system to possess a substantial atmosphere, with a surface pressure ~50% greater than Earth's. Titan's atmosphere is composed of 98% N_2, ~2% CH_4, and small amounts of complex organic molecules formed from photochemical reactions in the atmosphere. These photochemical reactions destroy the atmospheric methane, transforming it into heavier organic molecules which then precipitate onto the surface. These organic molecules form Titan's liquid hydrocarbon lakes and seas in the polar regions, and the dunes in the equatorial regions. Underneath Titan's icy surface, evidence suggests the existence of a subsurface water ocean (Sohl et al. 2014). Since organics and water play an essential role in life on Earth, Titan's organic molecules and subsurface water ocean make Titan an astrobiologically interesting target. Assuming organics from the atmosphere and surface could interact with the water ocean and produce biosignatures (Neish et al., 2009; Brassé et al., 2017), how could they be delivered up to the surface for detection? One such mechanism is cryovolcanism (Lopes et al., 2013).

Cryovolcanism involves the eruption of molten material with low melting points from the interiors of icy satellites. Analogous to terrestrial volcanism in which molten rock is the magma, the cryomagma is liquid water or a water–ice slurry. There is evidence of cryovolcanic resurfacing on other icy bodies in the solar system, for example, the plumes emanating from Enceladus's south pole (Porco et al., 2006), and the young surface and possible plumes of Europa (Zahnle et al., 2003, Roth et al., 2014). The NASA Cassini mission's visible, near-infrared, and radar imaging of Titan's surface has revealed potential

cryovolcanic features such as effusive flows and domes (Lopes et al. 2013). Although Titan seems to be predominately resurfaced by fluvial and aeolian processes (Lopes et al. 2019), cryovolcanism is likely responsible for at least some surface features (Lopes et al. 2013), and several authors have proposed mechanisms by which cryovolcanic resurfacing could take place (Fortes et al. 2006, Mitri et al. 2008, Sohl et al. 2014). In this study, we investigate pressure-driven effusive cryovolcanism as a transport mechanism for liquids contained in discrete reservoirs within Titan's ice shell. Such reservoirs may be emplaced by liquid driven upwards from the ocean by the exsolution of volatiles in cracks initiated at the base of the ice shell (Crawford and Stevenson, 1988). Other possibilities include melting associated with convection in the ice shell, which could transport heat and chemicals (Head and Pappalardo, 1999), or partial melting of the ice by tidal dissipation (Mitri and Showman, 2008); both mechanisms might lead to warm ice or melt pockets near the surface. Regardless of formation mechanism, it is proposed that the water in the reservoir expands upon freezing and develops a critical pressure high enough to fracture the reservoir walls and drive fluid to the surface (Fagents 2003, Lesage et al., 2020).

A recent study for Europa showed that eruptions can be produced by the freezing of pure water and briny liquid contained in spherical reservoirs with radii between 60 and 1300 m located at depths between 1 and 10 km in the ice shell (Lesage et al. 2020). In this MS project, we develop a mathematical model for Titan conditions, following Lesage et al. (2020), to address the following objectives: (1) calculate the volume fraction of the reservoir that needs to freeze to generate the critical reservoir pressure to produce an eruption, (2) calculate the time required for that degree of freezing to be achieved, and (3)

determine the volume of erupted material, all as a function of reservoir depth, volume, and liquid composition.

The composition of Titan's subsurface ocean is unknown, but models suggest it may be composed of pure liquid water, a water–ammonia mixture, or an ammonium sulfate–water mixture (Fortes et al. 2006; Sohl et al. 2014). For this project, we will explore all three and compare the resulting eruption processes. The water–ammonia mixture contains 1.5 wt.% ammonia, the maximum amount thought to be contained in Titan's subsurface ocean (Tobie et al., 2012). We explore concentrations of 10 and 20 wt.% ammonium sulfate, which was proposed by Fortes et al. (2006) to be a substantial component of the ocean. We compare freezing times with timescales of gravity-driven subsidence of the water body through the ice to evaluate the feasibility of our model. We also evaluate presumed reservoir volumes based on the size of resolvable flow-like features imaged by the Cassini mission to explore the feasibility of subsurface liquid reservoirs as a potential resurfacing mechanism on Titan.

2 Methods

The cryovolcanic mechanism proposed is as follows. We assume a cryomagma reservoir exists within the brittle portion of the ice shell at an initial temperature, pressure, and volume, T_i, P_i, V_i, respectively, as shown in Figure 1. The cold surrounding ice (at temperature T_c) cools the cryomagma to its freezing point and then the cryomagma begins to freeze. Because the density of liquid water ρ_l is greater than that of solid ice ρ_s, the pressure in the reservoir increases as the phase change progresses. We assume no elastic or ductile

accommodation by the reservoir walls during this freezing stage (Lesage et al., 2020). The pressure increases until a critical pressure ΔP_c is met, analogous to terrestrial magma chambers that fracture when the tensile stresses exceed the tensile strength of the surrounding rock (McLeod and Tate, 1999).

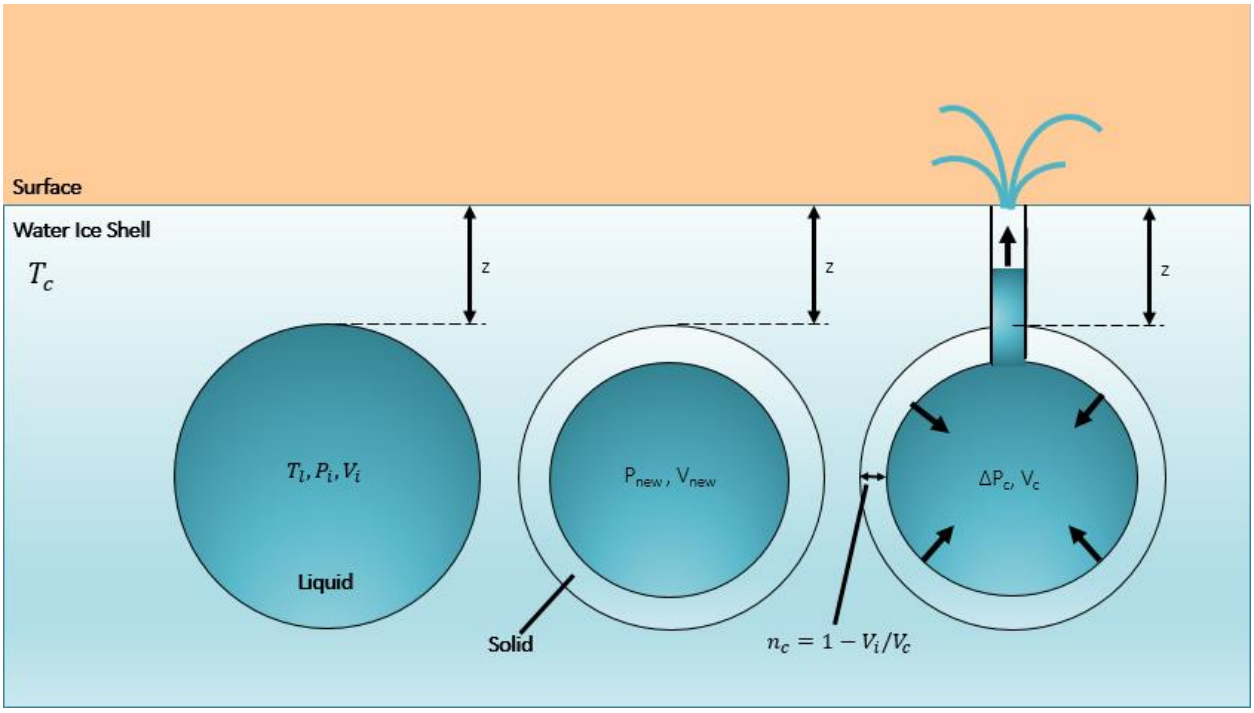

Figure 1. Illustration of eruption mechanism. (1) The reservoir exists at some depth in the ice shell at an initial temperature T_i, pressure P_i, and volume V_i. (2) The cryomagma changes phase producing a volume of ice and reducing the remaining liquid volume to V_c; the resulting density change increases the pressure in the reservoir to P_{new}. (3) A critical pressure ΔP_c is reached that fractures the surrounding ice and erupts.

Reservoir geometries are unconstrained for Titan, so we assume a spherical liquid reservoir. Since liquid water is denser than water ice, the reservoir's residence time in the ice shell is limited, because gravity might induce downward motion of the water via percolation or wholesale subsidence of the reservoir (Kalousová et al., 2016). If eruption of fluid at the

surface is to be possible, the critical freezing time must be less than the time it takes liquids to move downwards in the ice shell, an issue we address later in the Discussion section. Possible depths of reservoirs are also unconstrained for Titan, so we explore a range of depths. Titan's ice shell is ~110 km thick (Sohl et al., 2014); however, our model necessitates that we investigate only the portion of the ice shell that behaves elastically. The thickness of the brittle ice shell is likely 30 – 40 km (Schurmeier and Dombard, 2018). Therefore, in this study we assume that Titan's ice shell behaves elastically to depths of 30 km in order to facilitate comparison of our model to the results presented for Europa in Lesage et al. (2020).

Before the liquid changes phase, the removal of heat by convection within the reservoir cools the liquid to its solidification point (Craft et al. 2016, Lesage et al., 2020)

$$\tau_{cooling} \approx \rho_l R\, c_p \Delta T / q_{loss} \quad (1)$$

where ΔT is the difference between the initial temperature and the melting temperature, R is the reservoir radius, c_p=4 x 10^3 J kg^{-1} K^{-1} is the liquid water heat capacity, q_{loss} is the convective heat loss of the liquid, given by

$$q_{loss} \approx k_l \Delta T Ra^{1/3} / R \quad (2)$$

and k_l=0.6 W m^{-1} K^{-1} is the liquid water thermal conductivity. The Rayleigh number Ra is given by

$$Ra = g\, \rho_l\, \alpha\, R^3 \Delta T / (\mu \kappa_l) \quad (3)$$

where g is the acceleration due to gravity (1.35 m s^{-2} for Titan), and κ_l is the thermal diffusivity of the liquid.

The initial temperature of the liquid is unlikely to be much higher than the melting point so we take $\Delta T = 1\ K$. The dynamic viscosity of liquid water is 10^{-3} Pa s, and assume this as the value for the 1.5 wt.% NH_3-H_2O mixture as well, since the concentration of ammonia is low. Equation (1) gives a cooling time to the freezing point of ~4 – 160 days for the smallest and largest reservoirs examined. The dynamic viscosities of the 10 and 20 wt.% ammonium sulfate mixtures are 2.1 x 10^{-3} Pa s and 2.8 x 10^{-3} Pa s; cooling times of these cryomagmas are, respectively, 12 hours to 20 days and 4 hours to 6 days for the range of reservoir depths investigated, i.e., $\sim 1/8^{th}$ and $1/27^{th}$ of the pure water cooling times.

2.1 Freezing and fracture of cryomagma reservoir

Here we describe the governing equations of our model, following Lesage et al. (2020). The overpressure in the reservoir from the compression of the liquid is what initiates and drives the eruption. It depends on the liquid compressibility χ, given by

$$\chi = -\frac{1}{V}\frac{\partial V}{\partial P} \qquad (4)$$

where V is the volume and P is the pressure of the liquid. We consider a constant compressibility, so the overpressure in the reservoir is

$$\Delta P = -\frac{1}{\chi} l\,n\left(\frac{V_f}{V_i}\right). \qquad (5)$$

This overpressure creates the tensile stress on the reservoir wall that initiates eruption, given by (McLeod and Tait, 1999)

$$\sigma_{\theta\theta} = \sigma^0 \left[1 + \frac{1}{2}\left(1 - \frac{P_{tot}}{\sigma^0}\right)\right] \quad (6)$$

where σ^0 is the lithostatic pressure of the ice shell and P_{tot} is the total pressure in the reservoir, given by

$$P_{tot} = \rho_s g z + \Delta P \quad (7)$$

Compressive stress is taken to be positive so the tensile failure occurs when

$$\sigma_{\theta\theta} \geq -\sigma_c \quad (8)$$

where σ_c is the critical value. Combining Equations (6), (7), and (8) we derive the equation for the critical overpressure

$$\Delta P_c = 2(\sigma_c + \rho_s g z) \quad (9)$$

where σ_c is the tensile strength of the ice (McLeod and Tate 1999, Lesage et al. 2020). We use a linear relationship between the tensile strength of ice and temperature that was experimentally derived in Litwin et al. (2012): $\sigma_c = 2.4 \times 10^6 - (0.0073 \times 10^6)\ T_c$, where T_c is the temperature of the ice shell. The ice shell temperature is given by

$$T_c = T_s \exp\left(\frac{qz}{651}\right) \quad (10)$$

where T_s is the surface temperature of Titan, z is the depth, and q is the surface heat flow. We consider two heat flows, q = 3 mW/m^2 and q = 7mW/m^2 (Tobie et al. 2004) in order to observe the effect of ice shell temperature on our eruption model.

To find the critical freezing fraction and time required to induce reservoir failure and initiate fluid ascent and eruption, we solve the one-dimensional heat conduction equation for the position of the phase-change boundary (the Stefan problem; Turcotte and Schubert, 2014) between the liquid and newly-frozen ice in the reservoir. We assume that the temperature at the interface between the reservoir and the surrounding ice is the same at every point of contact around the spherical reservoir. Following Lesage et al. (2020), we calculate the critical fraction of cryomagma required to reach the critical pressure to induce reservoir failure

$$n_c = \frac{\exp\left(\chi \Delta P_c\right) - 1}{\frac{\rho_l}{\rho_s}\exp\left(\chi \Delta P_c\right) - 1} \tag{11}$$

where χ is the compressibility of the liquid and ΔP_c is the critical pressure, given by Equation (9).

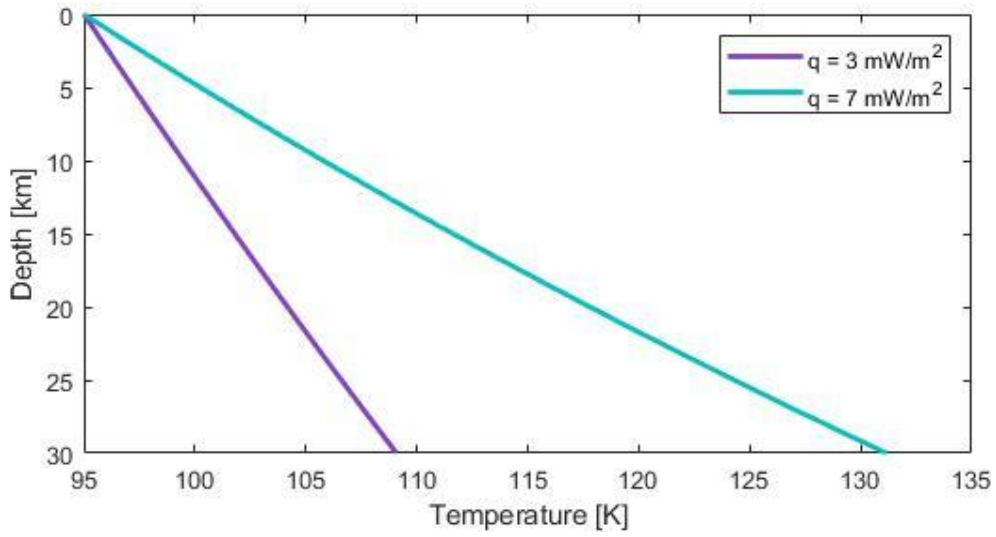

Figure 2. Thermal profiles of Titan's ice shell for two heat flow values, 3 mW/m^2 (purple curve) and 7 mW/m^2 (cyan curve) given by Equation (10). The temperature difference between the two heat flow values increases with depth in the ice shell.

The position of the freezing front can be written as a function of the reservoir radius and freezing fraction

$$S_c = R(1 - (1 - n_c)^{1/3} \quad (12)$$

and a critical freezing time can be deduced from the resulting relationship

$$\tau_c = (\frac{S_c}{2\lambda\sqrt{\kappa_s}})^2 \quad (13)$$

where κ_s is the ice thermal diffusivity and λ is a dimensionless parameter (Turcotte and Shubert, 2014). The dimensionless parameter λ is found numerically, by iterating through the possible solutions and finding a match with the right hand side of the following equation

$$\lambda(1 + erf\lambda) \exp \lambda^2 = \frac{(T_l - T_c)c_p}{L\sqrt{\pi}} \quad (14)$$

where T_l is the temperature of the liquid, T_c is the temperature of the surrounding ice, c_p is the heat capacity of water ice, and L is the latent heat of fusion of water. This equation comes from the one-dimensional heat conduction equation, solved in Cartesian coordinates.

2.2 Eruption parameters

In this section we derive the equations that govern the amount of material erupted and the duration of these events. Once a fracture has opened, the initial flow velocity U is calculated from the initial overpressure ΔP_c and the volume of the remaining liquid in the reservoir

$$V_f = (1 - n_c \frac{\rho_l}{\rho_s})V \quad (15)$$

where V_f is the volume of liquid after freezing, n_c is the critical freezing fraction, and V is the total volume of the reservoir. The velocity is calculated assuming turbulent flow using

$$U = \sqrt{\frac{D_h(P_{tot} - \rho_l g z)}{2 f z \rho_l}} \quad (16)$$

where D_h is the hydraulic diameter of the fracture or conduit, z is the depth of the reservoir, and f is the Fanning friction factor. The Fanning friction factor depends on the conduit properties; we assume a mean value of 0.01 (Lesage et al. 2020). The total pressure is given by Equation (7). Once the eruption begins, the pressurized cryomagma decompresses and the resulting fluid expansion continues to drive fluid ascent and eruption. In each increment of time, the volume of the fluid increases and the density of the fluid decreases. The overpressure due to the compressibility of the liquid is given by

$$\Delta P = \frac{-1}{\chi} ln(V_{new}/V_{old}) \quad (17)$$

where χ is the compressibility of the fluid, V_{new} is the new (expanded) volume of liquid, and V_{old} is the old (compressed) volume of liquid.

The decompressed volume achieved after each time step is calculated by adding V_{old} to the effusion rate multiplied by the time step size

$$V_{new} = V_{old} + A\, U_{old}\, dt \quad (18)$$

where A is the cross-sectional area of the conduit, U_{old} is the velocity calculated during the previous time step, and dt is the time step. The change in reservoir total pressure with time

Table 1. Model parameters

Definition	Symbol	Value	Units	Reference
Liquid density (H_2O)	ρ_l	1000	kg m^{-3}	Kargel (1991)
Liquid density (1.5 w.% NH_3-H_2O)		993		Croft et al. (1988)
Liquid density (10 w.% NH_4SO_4-H_2O)		1050		Fortes et al. (2006)
Liquid density (20 w.% NH_4SO_4-H_2O)		1125		Fortes et al. (2006)
Water ice density	ρ_s	920		Kargel (1991)
Melting temperature (H_2O)	T_l	273	K	Lesage et al. (2020)
Melting temperature (1.5 w.% NH_3-H_2O)		272		Croft et al. (1988)
Melting temperature (10 w.% NH_4SO_4-H_2O)		272		Fortes et al. (2006)
Melting temperature (20 w.% NH_4SO_4-H_2O)		268		Fortes et al. (2006)
Heat capacity of water ice	c_p	2 x 10^3	J kg^{-1} K^{-1}	Hobbs (1975)
Heat capacity of liquid water		4 x 10^3	J kg^{-1} K^{-1}	Fortes et al. (2006)
Thermal conductivity of liquid water	k_l	0.6	W m^{-1} K^{-1}	Blumm and Lindemann (2003)
Acceleration of gravity	g	1.35	m s^2	
Liquid water thermal expansion coefficient	A	10^{-3}	K^{-1}	Craft et al. (2016)
Dynamic viscosity (H_2O and 1.5 w.% NH_3-H_2O)	μ	10^{-3}	Pa s	Hillier and Squires (1991)
Dynamic viscosity (10 w.% NH_4SO_4-H_2O)		2.1 x 10^{-3}	Pa s	Fortes et al. (2006)
Dynamic viscosity (20 w.% NH_4SO_4-H_2O)		2.8 x 10^{-3}	Pa s	Fortes et al. (2006)
Liquid water thermal diffusivity	κ_l	10^{-7}	m^2 s^{-1}	Craft et al. (2016)
Liquid water compressibility	X	5 x 10^{-10}	Pa^{-1}	Fine and Millero (1973)
Ice thermal diffusivity	κ_s	$\kappa_s = k_s / \rho\ c_p$	m^2 s^{-1}	Craft et al. (2016)
Water ice thermal conductivity	k_s	2.3	W m^{-1} K^{-1}	Hobbs (1975)
Temperature difference between ice shell and reservoir	ΔT	1	K	Lesage et al. (2020)

is given by

$$P_{tot,new} = P_{tot,old} - \frac{1}{\chi} ln(V_{new}/V_{old}) \quad (19)$$

where the subscripts 'new' and 'old' refer to the volumes and pressures at the current and previous time steps. As the eruption proceeds, the volume of liquid continues to expand until the reservoir total pressure is balanced by the hydrostatic pressure due to the column of fluid in the conduit.

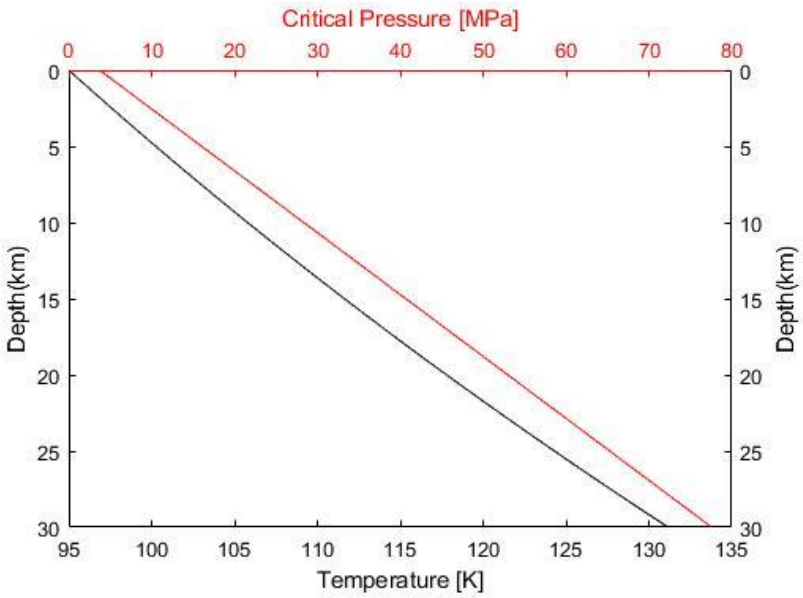

Figure 3. Plot showing temperature given by Equation (10) and critical pressure given by Equation (9) as a function of depth. The bottom x-axis shows the temperature of the ice for the upper 30 km of Titan's ice shell. The top x-axis shows the critical pressure, the pressure that a freezing reservoir must reach for an eruption to occur, as a function of depth.

The nature of the flow (turbulent vs. laminar) depends on the Reynolds number

$$Re = \frac{\rho_l U b}{\mu} \quad (20)$$

where b = 1 m is the fracture width and μ is the liquid dynamic viscosity, given in Table 1. We choose a rectangular fracture with a cross-sectional area of 100 m^2 and perimeter of 200 meters, after Lesage et al. (2020). This fracture geometry was chosen arbitrarily since geometries are unconstrained for fractures on Europa, as on Titan. The nature of the flow will be discussed in the following section.

3 Results

3.1 Freezing

The critical freezing fraction depends on the critical pressure necessary to fracture the surrounding ice. We consider pure water, a 1.5 wt.% ammonia–water mixture, and 10 and 20 wt.% ammonium sulfate–water mixtures. The density and melting temperature of the ammonia–water mixture were found using the equation of state derived in Croft et al. (1988) and are given in Table 1. Note that these values are very close to the density and melting temperature of pure water; 1000 kg/m^3 and 273 K. The aqueous ammonium sulfate parameters are also given in Table 1. Following Lesage et al. (2020), we assume all compositions have the same thermal conductivity and heat capacity as pure water, as these properties vary little at these concentrations (Che et al., 2012, Fortes et al., 2006).

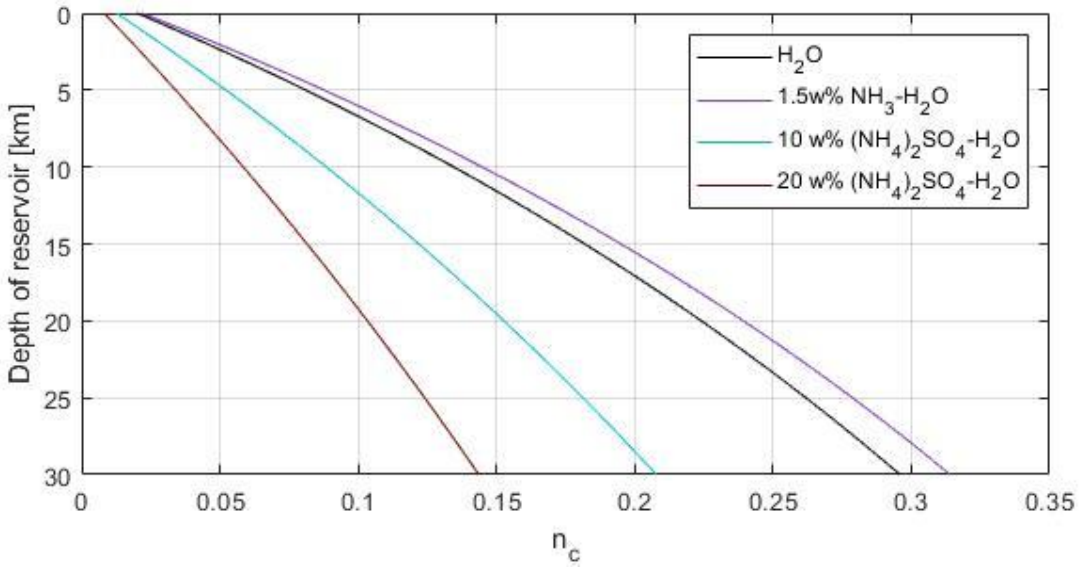

Figure 4. The critical freezing fraction as a function of depth, calculated using Equation (11). Note that the critical freezing fraction is independent of reservoir size. The teal line is the 10 wt.% ammonium sulfate–water mixture, the brown line is the 20 wt.% ammonium sulfate–water mixture, the black line is pure water, and the purple line is the 1.5 wt.% ammonia–water mixture.

The results are shown for all cryomagma compositions in Figure 4. The critical freezing fraction increases with depth since the lithostatic pressure term dominates the critical pressure (see Equation 8). For a pure water cryomagma reservoir in the brittle ice shell, the fraction of the reservoir that must freeze is between 2 and 28% to cause the critical pressure necessary to fracture the surrounding ice shell, 3.7 – 77.6 MPa (Figure 3). The freezing fraction increases for the 1.5 wt.% ammonia–water cryomagma (density 993.2 kg/m^3), between ~2 and 32%. The critical freezing fraction for the 10 wt.% ammonium sulfate cryomagma (density 1050 kg/m^3) is ~1 – 14%, and for 20 wt.% ammonium sulfate (density 1125 kg/m^3) is ~2 – 21%.

The times required to achieve the critical freezing fraction for the variety of reservoir sizes considered in this study are shown in Figure 5 as a function of reservoir depth. Pure water and ammonia–water take tens of years to 10^4 years for the smallest and largest reservoirs. The 20 wt.% ammonium sulfate cryomagma freezing times are an order of magnitude smaller than those of pure water and ammonia–water for all reservoir conditions. The density change on changing phase from liquid to solid provides the driving pressure gradient for the eruption, so the greater the density contrast between the cryomagma and its solid counterpart (water ice, density = 920 kg/m^3), the faster a reservoir can reach the point of eruption. This is why the results for the two ammonium sulfate compositions differ so markedly from the pure water case, the density contrast between aqueous ammonium sulfate and water ice ($\Delta\rho$ = 130 – 205 kg/m^3) is substantially greater than that of the pure water ($\Delta\rho$ = 80 kg/m^3) or ammonia–water ($\Delta\rho$ = 73 kg/m^3) with respect to water ice.

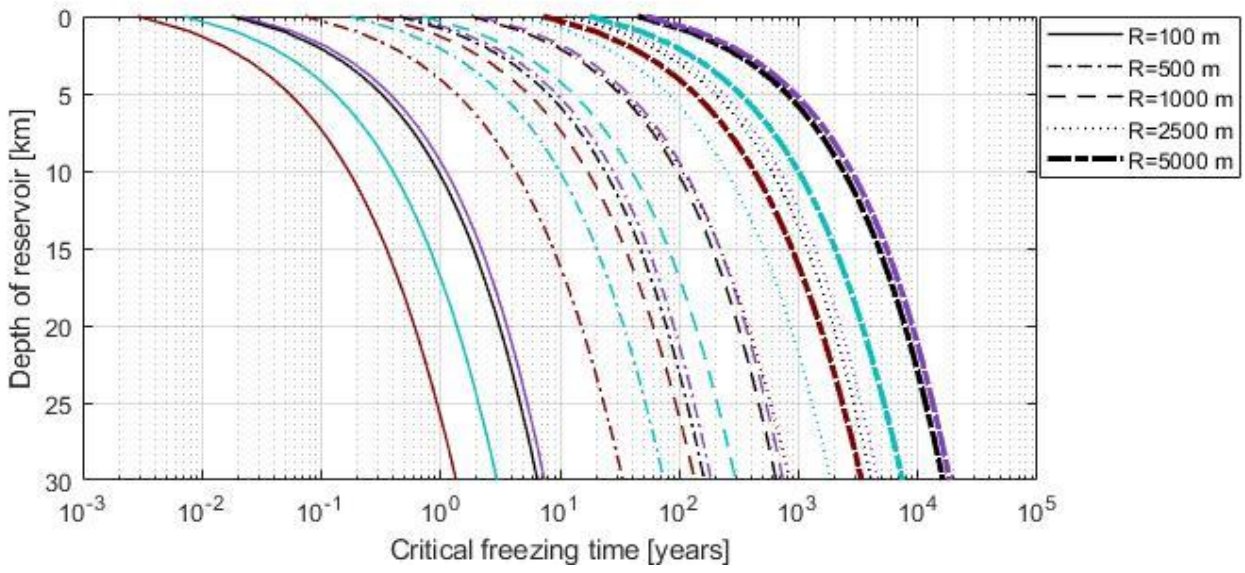

Figure 5. The freezing time required to achieve the critical freezing fraction as a function of reservoir depth in the ice shell (Equation 13), for the warmer temperature profile (heat flow = 7 mW/m^2) calculated by Equation

(10). Black = pure water, purple= 1.5 wt.% ammonia–water mixture, teal = 10 wt.% ammonium sulfate–water mixture, brown= 20 wt.% ammonium sulfate–water mixture. The thin solid line corresponds to a reservoir radius R=100 m, dotted line to R=500 m, dashed line to R=1000 m, dashed-dotted line R=2500 m, and thick solid line to R=5000 m.

3.2 Eruption

Once the critical freezing fraction (and hence the critical overpressure) has been achieved, the ice fractures, the reservoir fluid decompresses, and the fluid is driven up the conduit to erupt at the surface. The eruption ceases when the cryomagma ascent velocity reaches zero, which occurs when the hydrostatic pressure of fluid in the conduit balances the remaining excess pressure in the reservoir. For all depths explored, the eruption durations are nearly identical between the pure water and ammonia–water cryomagmas, ranging from a few seconds to 5000 hours. For a given reservoir size, the volume of erupted cryomagma is the same order of magnitude for all four cryomagma compositions. For the range of reservoir sizes modeled, we find eruption volumes of 10^4 – 10^{10} m^3, as shown in Figure 6. An interesting feature to note is that only 14% of the 20 wt.% ammonium sulfate cryomagma must freeze in order to produce the same amount of erupted material as the same sized reservoir with pure water cryomagma, which requires 30% of the reservoir to freeze. This is because the eruption is driven by the overpressure and both eruptions must begin at the same critical pressure, which is more readily achieved for a denser cryomagma with a larger density contrast between the liquid and solid phases.

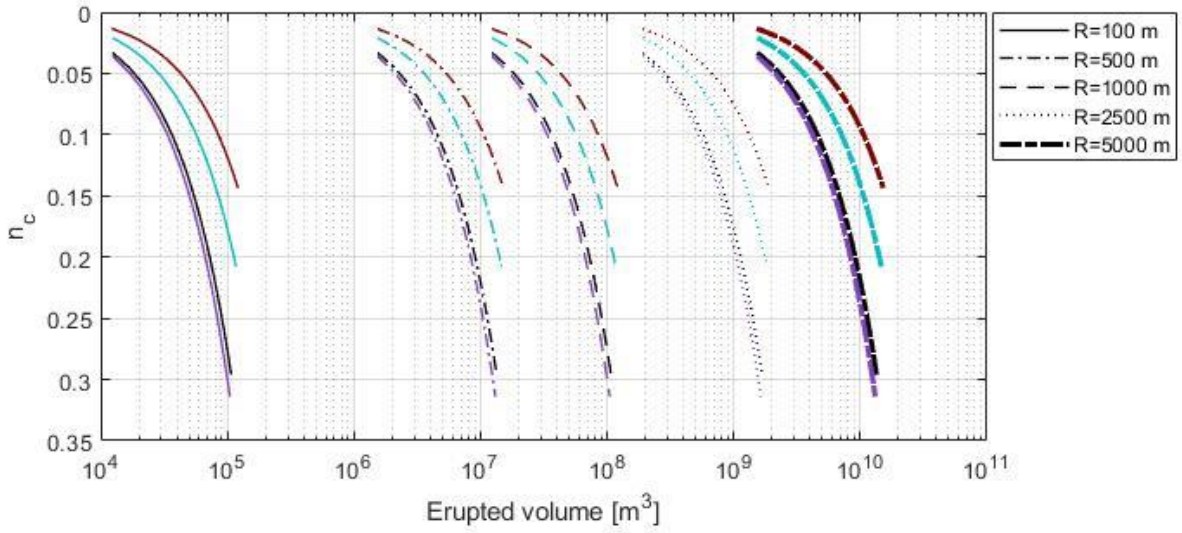

Figure 6. Plot of volume of erupted cryomagma for all reservoir sizes and their corresponding critical freezing fractions n_c, which increase with depth. Black = pure water, purple= 1.5 wt.% ammonia–water mixture, teal = 10 wt.% ammonium sulfate–water mixture, brown = 20 wt.% ammonium sulfate–water mixture. The thin solid line corresponds to a reservoir radius R=100 m, dotted line to R=500 m, dashed line to R=1000 m, dashed-dotted line R=2500 m, and thick solid line to R=5000 m.

The results presented in this study are for a fracture or conduit with hydraulic diameter D_h=2 in Equation (16), after Lesage et al. (2020). We also calculated the results for a hydraulic diameter of D_h=4, essentially doubling the crack width. This increases the initial eruption velocity and decreases the eruption duration. However, we neglect eruption durations in our discussion of eruption times because they are on the order of hours, significantly less than the freezing times.

The assumption that the flow is turbulent can now be verified using equation (16) and the results shown in Figure 7. At the beginning of the eruption, the flow velocity is 16 m/s for the pure water and 1.5 wt.% ammonia–water cryomagmas, which corresponds to a Reynolds number of 10^7. The Reynolds number is not significantly different for the

ammonium sulfate compositions, since the initial velocity is 14 – 15 m/s and the small differences in density and viscosity compensate for each other in Equation (20). The laminar regime (Re < 1000) is not reached until the velocity reaches 10^{-3} m/s, which happens only at the end of the eruption.

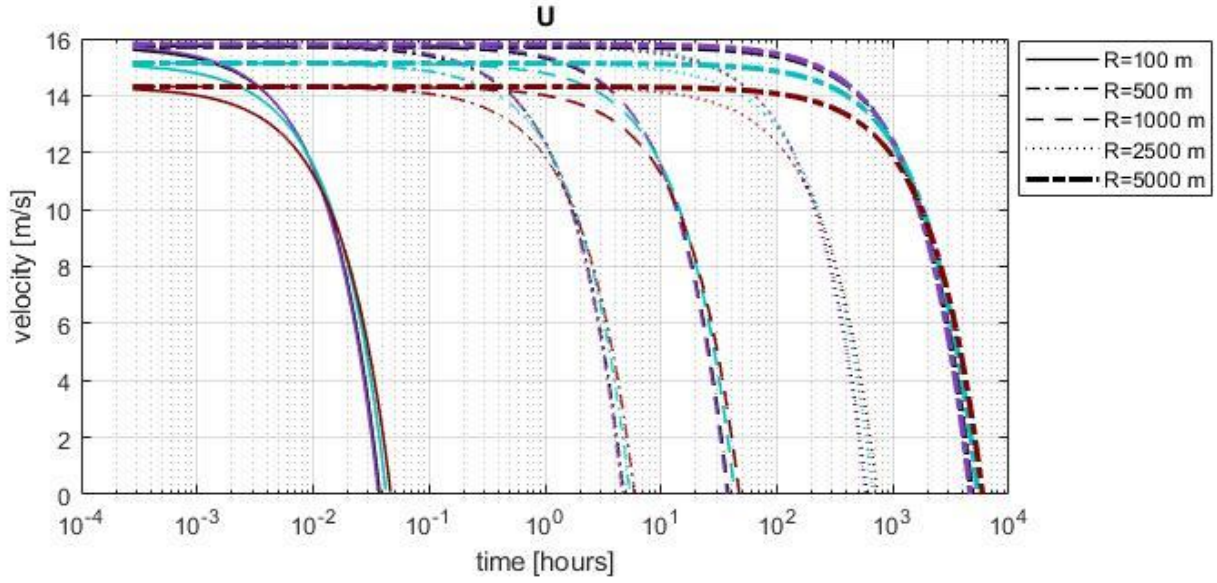

Figure 7. Variation of the velocity, given by Equation (16), of the erupting material with time for reservoirs at 10 km depth, for the warmer ice shell temperature profile (heat flow = 7 mW/m^2). The eruption ends when the velocity reaches zero. Black = pure water, purple= 1.5 wt.% ammonia–water mixture, teal = 10 wt.% ammonium sulfate–water mixture, brown= 20 wt.% ammonium sulfate–water mixture. The thin solid lines correspond to a reservoir radius R=100 m, dotted lines to R=500 m, dashed lines to R=1000 m, dashed-dotted lines R=2500 m, and thick solid lines to R=5000 m.

3.2 Effect of ice shell temperature

Figure 2 shows the thermal profiles for both the cold and warm ice shells (heat flows of 3 and 7 mW/m^2, respectively) considered in the modeling. Although the temperature differs significantly at depth between the two ice shells, the temperatures for depths we are

interested in (<30 km) vary by a maximum of ~20 K. The freezing fractions remain similar with respect to the order of magnitude estimates we are making. A noticeable difference, however, is the freezing times. Comparison of Figure 5 and Figure 8 reveal that the ice shell with a heat flow assumption of 3 mW/m^3 decreases the freezing time of reservoirs (relative to the 7 mW/m^3) by a maximum of 15%, occurring at a depth of 30 km. The difference in freezing time decreases with decreasing depth, since the temperature profiles for the two heat flow assumptions (Figure 2) are closest at shallow depths within the ice shell.

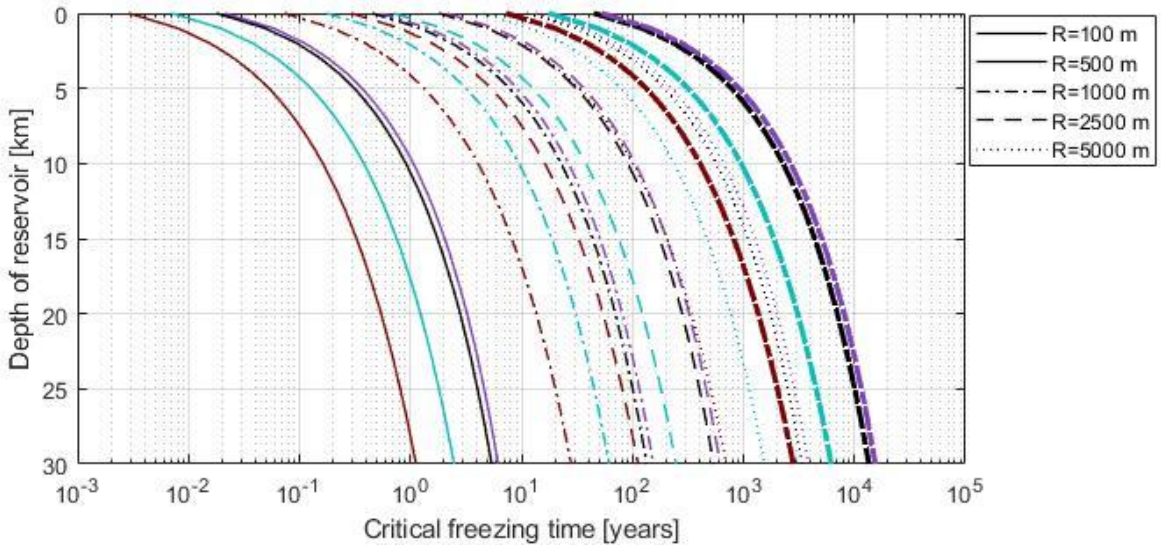

Figure 8. Freezing times required to achieve the critical freezing fraction (Equation 8) for an ice shell with heat flow 3mW/m^2 (Equation 9). Black = pure water, purple= 1.5 wt.% ammonia–water mixture, teal = 10 wt.% ammonium sulfate–water mixture, brown= 20 wt.% ammonium sulfate–water mixture. The thin solid line corresponds to a reservoir radius *R*=100 m, dotted line to *R*=500 m, dashed line to *R*=1000 m, dashed-dotted line *R*=2500 m, and thick solid line to *R*=5000 m.

3 Discussion

4.1 Downward movement of reservoirs

In order for a subsurface fluid reservoir to produce an eruption, it must remain stable during the freezing process. However, gravity acting on cryomagma reservoirs may cause them to subside downwards through the ice shell, since the cryomagmas are denser than solid water ice. This means that, for an eruption to take place from a subsurface fluid reservoir, the freezing and eruption timescales must be substantially less than the downward transport time of fluid out of the elastic shell. Kalousova et al. (2016) modeled the lifetimes of partially molten regions of negative buoyancy formed under strike-slip faults in the ice shell of Europa. In their model the timescales of downward movement are controlled by the timescale of formation of a Rayleigh-Taylor instability and the rate at which the fluid migrates downward through the ice shell due to the viscous flow of the surrounding ice. We do not attempt to directly compare our results to their downward transport times, because the ice shell of Europa is warmer than Titan's, and therefore more conducive to downward migration of fluids. Rather, we cite their study as an approach that could be taken in future work to further test the feasibility of our model as an eruption mechanism on Titan.

However, we can derive a first-order estimate of the transport time by considering Stoke's law, which describes the terminal velocity of a sphere (i.e., the reservoir in our case) moving through a viscous medium (i.e., the ice)

$$v = \frac{2(\rho_l - \rho_s)}{9\mu_{ice}} gR^2 \qquad (21)$$

where ρ_l is the density of the cryomagma , ρ_s is the density of the ice shell, R is the reservoir radius, and μ_{ice} is temperature-dependent ice viscosity

$$\mu_{ice} = 10^{14} \exp\left\{25.2\left(\frac{273}{T(K)} - 1\right)\right\} \quad (22)$$

derived in Hillier and Squyres (1991). Considering both thermal profiles (3 and 7 mW/m^3) the range of viscosities relevant to our model is 10^{25} – 10^{34} Pa s, resulting in terminal velocities of 10^{-25} – 10^{-13} km/year, decreasing with increasing depth and size of reservoir. Multiplying the resulting velocities by the distance between the initial depth of the reservoir and the bottom of the elastic ice layer (z = 30 km) yields the time to reach the bottom of the elastic ice layer; between 10^{13} – 10^{26} years. Therefore, reservoir freezing times must be less than this time frame for eruptions to be possible. However, the local warming of the ice surrounding the reservoir is not accounted for in this calculation. The warming would locally decrease the viscosity, which could decrease subsidence times.

To put this time in to context, consider a reservoir of radius R=500 m. It produces the same amount of cryolava as that of potential flow features observed on Titan at Tui and Hotei Regio (Figures 9b & c); 10^6 – 10^7 m^3 (Barnes et al. 2006, Lopes et al. 2013) and takes ~10 – 200 years to freeze. Neglecting the local warming and viscosity decrease of the ice shell surrounding a reservoir, the downward movement time (10^{13} - 10^{26} years) is much greater than the time it takes to erupt. One of the most promising candidate cryovolcanic features on Titan is Doom Mons with its associated flow-like feature, Mohini Fluctus. We estimate that Mohini Fluctus (Figure 9a) has a volume of ~10^{11} m^3. Assuming the flow resulted from one eruption event, the most comparable eruption volume resulting from our model is the largest reservoir (R=5000 m). If the cryomagma is pure water, it can take between ~1000 and 10,000 years to freeze, still very much below the downward movement time. Alternatively, multiple successive eruptions from the same reservoir as freezing continues

to completion may produce such a flow, an idea which is explored for Europa in Lesage et al. (in press).

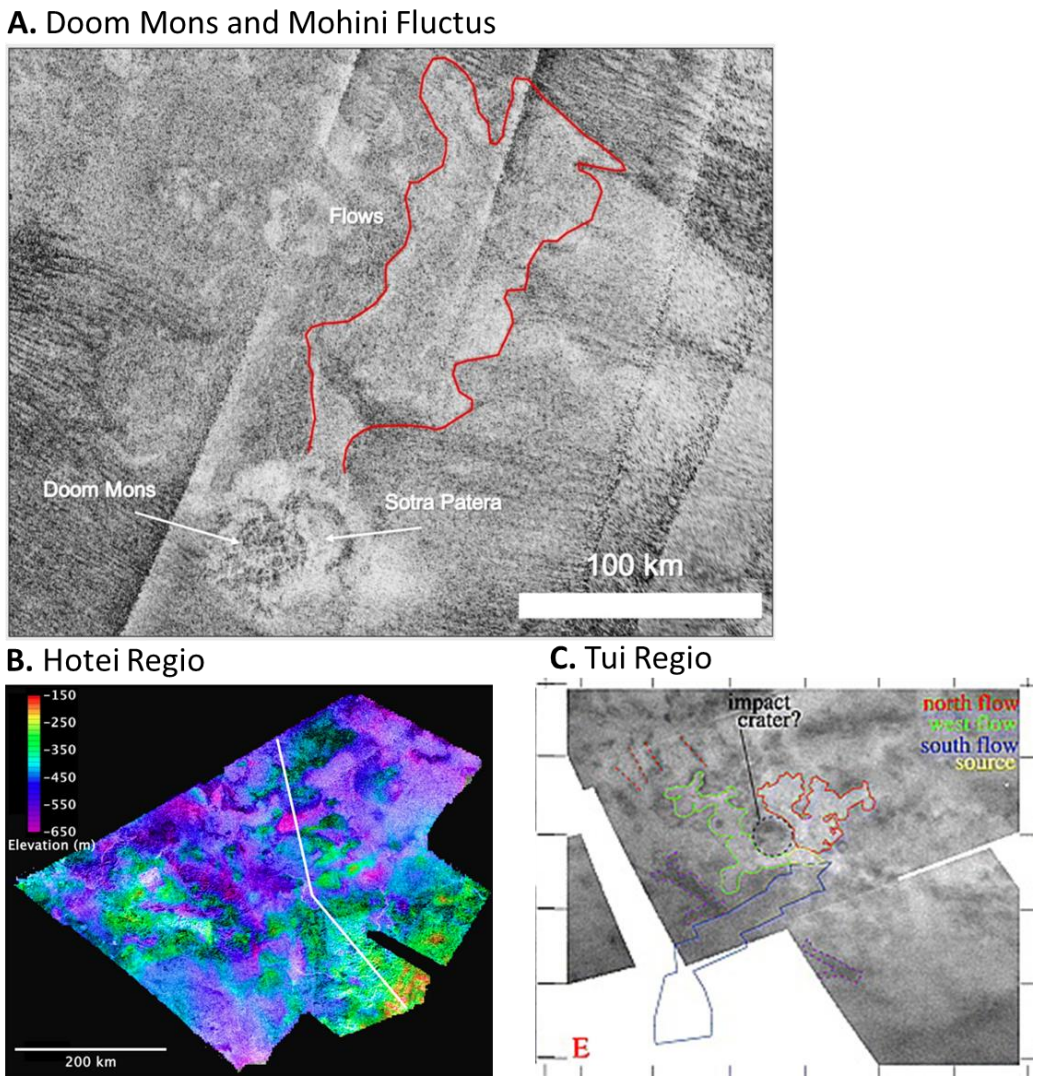

Figure 9. Three flow features on Titan used to compare model eruption volume results. Mohini Fluctus emanating from Doom Mons (a), 200 meter thick "flows" at Hotei Regio (b), and the "flows" at Tui Regio (c). (a) adapted from Werynski (2018), (b) adapted from Lopes et al. (2013) and (c) adapted from Barnes et al. (2006).

4.2 Stefan problem

We solve the Stefan problem in one dimension, assuming that the volume necessary to freeze is a thin layer compared to the reservoir radius. Hence this treatment is valid to give an order of magnitude estimate of the freezing time (Lesage et al. 2020). However, we find critical freezing fractions up to 32%. This high percentage prompts an assessment of the validity of using Cartesian coordinates for this model, which should be tested by solving the Stefan problem in cylindrical coordinates.

The Stefan problem solution requires that conditions satisfy the one-dimensional heat conduction equation (Turcotte and Schubert 2014). This requires that the properties of the solidified cryomagma and its surrounding ice are identical. Therefore, we assume that only pure water ice freezes out of the impure cryomagma solution. For simplicity we have neglected the changing concentration of ammonia or ammonium sulfate in the liquid phase as the water ice preferentially freezes out. In the case of ammonia, the increase in concentration could decrease the cryomagma density and freezing temperature. If this were explicitly modeled, the results could differ significantly for deeper reservoirs that require greater freezing fractions and times to reach the critical point. The freezing time depends on the temperature contrast and critical freezing fraction, and therefore the inverse of the ratio of the cryomagma density to ice. This is why the ammonium sulfate brine results in smaller freezing times. Here, our results differ from those of Lesage et al. (2020), who found that a freezing briny cryomagma would take longer to induce an eruption because they adopted a eutectic H_2O–$MgSO_4$–Na_2SO_4 composition, such that the sulfates freeze simulataneously with the ice, producing a salt-rich ice with density 1130 kg m^{-3}. The resulting density contrast between liquid and solid phases is only $\Delta\rho \sim 50$ kg/m^3,

which means a smaller volume change on freezing, and so a larger degree of freezing is required to achieve the critical pressure.

Accounting for the concentration change in the liquid phase during freezing could affect our results in the case of either ammonia or ammonium sulfate. Consider a reservoir of initial volume 10^{10} m^3; if the initial concentration of ammonia is 1.5% wt.% and the critical freezing fraction is 8%, once this critical fraction is achieved the cryomagma ammonia concentration has increased to 9.48 wt. % ammonia. The progressively increasing concentration during freezing would increase the density of the remaining liquid and decrease the solidification temperature, and hence act to increase the freezing time. In order to properly model a freezing reservoir with a concentration increase, the model would have to calculate the new concentration with every iteration of the phase change boundary before the critical position is met, changing the density and melting temperature of the cryomagma. Buffo et al. (2020) carried out a simulation of the freezing of Europa's ice shell and the subsequent evolution of the dissolved salt concentration using in part the analytical solution of the Stefan problem. In future work, the constitutive equations derived for their ice–ocean interface could be adapted to the conditions of our freezing spherical reservoir.

4.3 Ocean compositions

Cryovolcanic models often consider high ammonia concentrations in order to overcome the negative buoyancy issue of water (Mitri et al., 2008), but such high concentrations may not be realistic. Chemical models of Titan's subsurface ocean suggest an ammonia

concentration of 2 – 3 wt.% relative to water (Tobie et al., 2006); however, aqueous ammonia is very reactive with brine solutions (Kargel, 1992). Therefore, sulfate leaching from Titan's silicate core into the ocean will consume most of the free ammonia (Fortes et al., 2006). We entertained the possibility of a low-concentration ammonia–water ocean, but because ammonium sulfate may preferentially be present (Fortes et al., 2006), we considered two concentrations of ammonium sulfate–water mixtures. Fortes et al. (2006) developed a model for Titan's interior that requires an ocean concentration of up to 40 wt.% ammonium sulfate, which has a density of 1235 kg/m^3, substantially greater than that of water ice (920 kg/m^3). This eutectic composition would freeze directly to an ammonium sulfate hydrate ice mixture, therefore reducing the liquid–solid density contrast and inhibiting eruption. We therefore chose to investigate less concentrated solutions of 10 and 20 wt.% ammonium sulfate.

However, models for Titan's interior that suggest a dense subsurface ocean does not uniquely require the presence of ammonium sulfate. Other salts such as magnesium or sodium sulfates may be present (Kargel et al., 2000, Mitri et al., 2014). These salty oceans have densities as high as 1200 – 1400 kg/m^3 (Kargel et al., 2000). A cryomagma with density 1350 kg/m^3, the upper limit of Titan's subsurface ocean density according to Mitri et al. (2014), would result in even shorter freezing time scales than the ammonium sulfate–water cryomagmas explored in our model.

4.4 Elastic behavior of the ice shell

The assumption we made about the upper 30 km of Titan's ice shell behaving elastically, and the reservoir walls consequently remaining rigid, can be verified by calculating the Maxwell relaxation time of water ice. The Maxwell relaxation time provides timescales over which a material behaves elastically or viscously. It is given by

$$\tau_M = \frac{\mu_{ice}}{E} \quad (23)$$

where μ_{ice} is the temperature-dependent ice viscosity (Equation 22) and E is the Young's modulus of ice (~9 GPa; Petrenko and Whitworth, 2006). The maximum freezing time resulting from our model is $\sim 10^4$ years for the largest and deepest reservoir. Since this is faster than the Maxwell time computed, $\sim 10^8 - 10^{16}$ years, the ice deforms elastically for the ice shell temperatures explored in this study. However, this does not consider the heat transferred to the surrounding ice by the freezing reservoir which will decrease the local ice viscosity and ultimately decrease the Maxwell freezing time. This is outside the scope of our model, but will be important to consider in the future because it affects the behavior of the ice shell, the ability of reservoir walls to withstand pressurization without deforming, and the potential residence times of cryomagma reservoirs, as discussed in section 4.1.

5 Conclusion

We have shown that pressure-driven eruption of subsurface liquid reservoirs is a viable cryovolcanic mechanism for conditions relevant to Titan. The point of eruption for these reservoirs is easier to reach for smaller reservoirs, reservoirs located at shallower depths, and cryomagmas with larger density contrasts with respect to water. Freezing can occur

on timescales of months – 10^4 years for reservoirs with radii ranging from 100 – 5000 m residing in the brittle portion of the ice shell, containing cryomagmas of different compositions. The volume of liquid erupted ranges from ~10^4 – 10^{10} m^3, which is comparable to those of flow features observed on Titan (10^6 – 10^{11} m^3). We tested a warm (q=7 mW/m^2) and cool (q=3 mW/m^2) ice shell and found that freezing times are slightly longer for the warm ice shell.

We applied our model to four possible cryomagma compositions: 10 and 20 wt.% ammonium sulfate–water brine, 1.5 wt.% ammonia–water mixture, and pure water. The brine resulted in the shortest freezing times, doubling with the doubling of the concentration of ammonium sulfate. The 1.5 wt.% ammonia–water cryomagma freezing times are greater than pure water by a factor of ~2. Most previous models of cryovolcanism utilize ammonia to diminish the negative buoyancy barrier to cryogmagma ascent. However, this model of pressure-driven ascent suggests that ammonia hinders rather than promotes eruption at the surface. The composition of liquid reservoirs in Titan's ice shell is unlikely to be pure water, but as discussed in section 4, the concentration of impurities in the cryomagma would increase as the reservoir freezes. The next step in extending this work would be to appropriately model the temporal evolution of the cryomagma composition within the reservoir as water ice preferentially freezes out. Additionally, as discussed in section 4.2, the Stefan problem should be solved one dimensional radial geometry to test the validity of our solution in Cartesian coordinates.

6 References

Barnes, J.W., Brown, R.H., Radebaugh, J., Buratti, B.J., Sotin, C., Le Mouelic, S., Rodriguez, S., Turtle, E.P., Perry, J., Clark, R. and Baines, K.H., 2006. Cassini observations of flow-like features in western Tui Regio, Titan. *Geophysical Research Letters*, *33*(16).

Brassé, C., Buch, A., Coll, P. and Raulin, F., 2017. Low-temperature alkaline pH hydrolysis of oxygen-free Titan Tholins: carbonates' Impact. *Astrobiology*, *17*(1), pp.8-26.

Che, Y., Shen, J., Zhou, J., & He, C. (2012). Thermal Conductivity and Density of (NH4)2SO4 + H2O, NH4NO3 + H2O, and (NH4)2SO4 + NH4NO3 + H2O Solutions at T = (278.15 to 333.15) K. *Journal of Chemical & Engineering Data, 57*, 1486-1491.

Choukroun, M., Grasset, O., Tobie, G. and Sotin, C., 2010. Stability of methane clathrate hydrates under pressure: Influence on outgassing processes of methane on Titan. *Icarus*, *205*(2), pp.581-593.

Craft, K.L., Patterson, G.W., Lowell, R.P. and Germanovich, L., 2016. Fracturing and flow: Investigations on the formation of shallow water sills on Europa. *Icarus*, *274*, pp.297-313.

Fagents, S.A., 2003. Considerations for effusive cryovolcanism on Europa: The post-Galileo perspective. *Journal of Geophysical Research: Planets*, *108*(E12).

Fortes, A.D., Grindrod, P.M., Trickett, S.K. and Vočadlo, L., 2007. Ammonium sulfate on Titan: Possible origin and role in cryovolcanism. *Icarus*, *188*(1), pp.139-153.

Kargel, J.S., 1992. Ammonia-water volcanism on icy satellites: Phase relations at 1 atmosphere. *Icarus*, *100*(2), pp.556-574.

Kargel, J.S., Kaye, J.Z., Head III, J.W., Marion, G.M., Sassen, R., Crowley, J.K., Ballesteros, O.P., Grant, S.A. and Hogenboom, D.L., 2000. Europa's crust and ocean: origin, composition, and the prospects for life. *Icarus*, *148*(1), pp.226-265.

Kalousová, K., Souček, O., Tobie, G., Choblet, G. and Čadek, O., 2016. Water generation and transport below Europa's strike-slip faults. *Journal of Geophysical Research: Planets*, *121*(12), pp.2444-2462.

Lesage, E., Massol, H. and Schmidt, F., 2020. Cryomagma ascent on Europa. *Icarus*, *335*, p.113369.

Lesage, E. (2020). Etude du cryovolcanisme sur Europe. PhD thesis, University of Paris-Saclay, Manuscript submitted for publication.

Lopes, R.M., Kirk, R.L., Mitchell, K.L., LeGall, A., Barnes, J.W., Hayes, A., Kargel, J., Wye, L., Radebaugh, J., Stofan, E.R. and Janssen, M.A., 2013. Cryovolcanism on Titan: New results from Cassini RADAR and VIMS. *Journal of Geophysical Research: Planets*, *118*(3), pp.416-435.

McLeod, P. and Tait, S., 1999. The growth of dykes from magma chambers. *Journal of volcanology and Geothermal Research*, *92*(3-4), pp.231-245.

Mitri, G., Showman, A.P., Lunine, J.I. and Lopes, R.M., 2008. Resurfacing of Titan by ammonia-water cryomagma. *Icarus*, *196*(1), pp.216-224.

Mitri, G., Meriggiola, R., Hayes, A., Lefevre, A., Tobie, G., Genova, A., Lunine, J.I. and Zebker, H., 2014. Shape, topography, gravity anomalies and tidal deformation of Titan. *Icarus*, *236*, pp.169-177.

Neish, C.D., Somogyi, Á., Lunine, J.I. and Smith, M.A., 2009. Low temperature hydrolysis of laboratory tholins in ammonia-water solutions: Implications for prebiotic chemistry on Titan. *Icarus*, *201*(1), pp.412-421.

Petrenko, V.F. and Whitworth, R.W., 2006. Physics of Ice. NY.

Porco, C.C., Helfenstein, P., Thomas, P.C., Ingersoll, A.P., Wisdom, J., West, R., Neukum, G., Denk, T., Wagner, R., Roatsch, T. and Kieffer, S., 2006. Cassini observes the active south pole of Enceladus. *science*, *311*(5766), pp.1393-1401.

Roth, L., Saur, J., Retherford, K.D., Strobel, D.F., Feldman, P.D., McGrath, M.A. and Nimmo, F., 2014. Transient water vapor at Europa's south pole. *Science*, *343*(6167), pp.171-174.

Schurmeier, L.R., Dombard, A.J., Radebaugh, J. and Malaska, M., 2018. Intrusive and Extrusive Cryovolcanism and the Composition of Titan's Icy Crust. *LPI*, (2083), p.2934.

Sohl, F., Solomonidou, A., Wagner, F.W., Coustenis, A., Hussmann, H. and Schulze-Makuch, D., 2014. Structural and tidal models of Titan and inferences on cryovolcanism. *Journal of Geophysical Research: Planets*, *119*(5), pp.1013-1036.

Tobie, G., Grasset, O., Lunine, J.I., Mocquet, A. and Sotin, C., 2005. Titan's internal structure inferred from a coupled thermal-orbital model. *Icarus*, *175*(2), pp.496-502.

Tobie, G., Gautier, D. and Hersant, F., 2012. Titan's bulk composition constrained by Cassini-Huygens: implication for internal outgassing. *The Astrophysical Journal*, *752*(2), p.125.

Turcotte, D.L. and Schubert, G., 2014. Geodynamics. Third. 284-288.

Werynski, A., Neish, C.D., Le Gall, A., Janssen, M.A. and Cassini RADAR Team, 2019. Compositional variations of Titan's impact craters indicates active surface erosion. *Icarus*, *321*, pp.508-521.

Zahnle, K., Schenk, P., Levison, H. and Dones, L., 2003. Cratering rates in the outer Solar System. *Icarus*, *163*(2), pp.263-289.